THE JOURNAL OF PHYSICAL CHEMISTRY C

Article

pubs.acs.org/JPCC

Probing the Interfacial Charge-Transfer Process of Uniform ALD Semiconductor−Molecule−Metal Models: A SERS Study

Xiaolei Zhang,[†,‡] Yaoze Liu,[‡] Mohammad Soltani,[‡] Peng Li,[†] Bing Zhao,*[,†] and Bo Cui*[,‡]

[†]State Key Laboratory of Supramolecular Structure and Materials, Jilin University, Changchun 130012, P. R. China

[‡]Department of Electrical and Computer Engineering and Waterloo Institute for Nanotechnology (WIN), University of Waterloo, Waterloo, Ontario N2L 3G1, Canada

Supporting Information

ABSTRACT: Among all coating methods, atomic layer deposition (ALD), which can provide a precise thickness control at the angstrom or the monolayer level, appears to be one of the most promising techniques. To investigate the interfacial charge-transfer mechanism from semiconductor−molecule−metal systems, the order of different layers is very essential because the charge-transfer process can be affected by the interfacial contact order of different materials. Also, for TiO_2/MBA/Ag charge-transfer (CT) investigation, homogeneous assembling of TiO_2 with precisely controllable thickness is of great importance because the energy level of semiconductor is sensitive to its size at the nanoscale. Here, unlike previous 3D composite CT models, our semiconductor−molecule−metal interfacial CT models are fabricated with the ALD and e-beam evaporation techniques, which ensures the accuracy of the CT investigation. The surface-enhanced Raman scattering (SERS) technique is adopted in the investigation of the interfacial charge-transfer process through the changes of CT-sensitive bands. In TiO_2/MBA/Ag, the SERS signal of MBA molecules and the Raman spectra of TiO_2 phonon vibrational mode exhibit evident CT-driven changes. To confirm these phenomena, 4 nm thickness of wide-bandgap HfO_2 and Al_2O_3 are inserted as isolated layers. Also, the possible CT mechanisms and the charge-transfer degree in different systems are discussed. This work not only suggests a role for ALD in fabricating CT models but also promotes the application of SERS in more intensive fields.

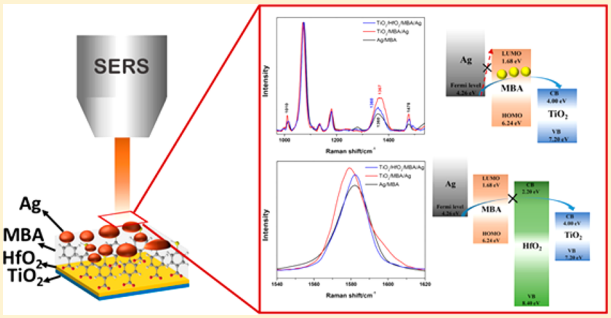

INTRODUCTION

Nowadays, due to its special photoelectric characteristics in optoelectronic devices, the semiconductor−molecule−metal system has led to a proliferation of studies as a widely used optoelectronic device model.[1−4] In these optoelectronic models, the charge-transfer(CT) properties of interfaces play a significant role in determining the performance of different photoelectric devices. Thus, a detailed investigation of the processes taking place between the layers is of crucial importance, which calls for highly uniform and preciously size-controlled CT models due to the sensitivity of nanoscale CT to the interfacial contact potential of different materials. With the innovation of traditional fabrication technology, the atomic layer deposition (ALD) technique, which provides a useful and powerful method for preparing uniform micro/nano film without pinholes, becomes increasingly noticeable.[5,6] Compared with other deposition methods, ALD can be easily used to precisely control the film thickness by the direct chemical reaction between the new atomic layer and the previous one, which suggests a role for ALD in CT system fabrication.

Besides the appropriate fabrication skill, a suitable experimental technique is also of great importance in CT investigation. X-ray photoemission (XPS),[7] resonant photoelectron spectroscopy (RPES),[8] transient absorption spectroscopy,[9] and many other techniques have usually been adopted in interfacial CT exploration. However, taking the sensitivity and time efficiency into account, more suitable experimental techniques are needed to achieve the in-depth understanding on the interfacial CT process as well as the significant improvement in photoelectric device performance. Surface-enhanced Raman spectroscopy (SERS) was first discovered in 1974 when the enhanced Raman signal of pyridine molecules was occasionally measured on a roughened silver electrode.[10] Over the past 40 years, SERS has made great progress due to the development of nanotechnology and excitation sources. Nowadays, due to its high selectivity, high sensitivity, and nondestructive nature, SERS has become a very powerful technique in many fields such as chemical analysis,[11] materials area,[12,13] biochemistry and biosensing,[14,15] electrochemistry,[16] and catalysis.[17] Two main mechanisms account for SERS: the electromagnetic mechanism (EM) and the chemical enhancement mechanism (CM). Among these two mechanisms, it is now generally agreed that the dominant contributor is EM,

Received: October 12, 2017
Revised: November 12, 2017
Published: November 15, 2017

ACS Publications © 2017 American Chemical Society

DOI: 10.1021/acs.jpcc.7b10086
J. Phys. Chem. C 2017, 121, 26939−26948

which results from the amplification of the light by the excitation of localized surface plasmon resonances (LSPRs).[18] Based on EM, many noble metal nanostructures are fabricated as ultrasensitive substrates. CM primarily involves a CT process between the substrate and the adsorbate in which the excitation wavelength is resonant with the metal−molecule charge-transfer electronic states.[19] Typically, in the SERS spectra the resonance CT process can increase the polarizability of probe molecules, which leads to enhancement in the Raman signal. With the function of CM, the involved CT process in the substrate/molecule system can be reflected in the corresponding SERS spectra by changing the polarizability of the adsorbed molecules.

To date, the SERS technique has been adopted to explore the CT process in different metal−molecule−semiconductor heterostructures. The charge-transfer direction and the charge-transfer degree in semiconductor−molecule−metal system are investigated with the SERS technique.[20,21] The CT processes in Ag/N719/TiO_2[22] and TiO_2/N3/Ag[23] dye-sensitized solar cell models are also studied with SERS spectra. In these works, although some SERS phenomena are deduced to come from the involved CT processes, it is difficult to definitely determine where these SERS changes come from and how the CT processes occur due to the disorder of different layer. Meanwhile, there is little report on highly uniform and precisely size-controlled models in investigation of CT process with SERS. Thus, more ordered models and more strong evidence are needed to evaluate and promote the application of the SERS technique in investigating interfacial CT processes.

In this work, we fabricated an ordered 2D semiconductor−molecule−metal charge-transfer system composed of anatase TiO_2, 4-mercaptobenzoic acid (MBA) molecule, and Ag island film on fused silica wafer. The TiO_2 film is fabricated with the ALD technique. After the absorption of MBA molecules on TiO_2 film with carboxyl group, the Ag island film is deposited with e-beam evaporation. Thus, the order of this semiconductor−molecule−metal CT system is fixed, which provides high uniformity for investigating the CT process. The MBA molecule between the semiconductor and metal works as both a linker and a SERS probe to reveal how charge transits in our system with SERS spectra. By comparing the changes of CT-sensitive bands in TiO_2/MBA/Ag and Ag/MBA, SERS enhancements derived from CT process are observed. Meanwhile, to verify the CT between TiO_2 and Ag, the wide-bandgap HfO_2 and Al_2O_3 are inserted by ALD. This work is conducive to both the renovation of CT model fabrication skill and the further investigation of the interfacial CT process in semiconductor−molecular−metal with the SERS technique.

EXPERIMENTAL METHODS

Chemicals. 4-Mercaptobenzoic acid (MBA) was purchased from Sigma-Aldrich and used without further purification. The ethanol was analytical grade.

Oxide Film Deposition by ALD. For all ALD processes, Ar was used as the purge gas between each half-reaction cycle. The film thickness was controlled by the numbers of the ALD cycles.

Deposition of Anatase TiO_2 Film. The TiO_2 is deposited on SiO_2 by the ALD process using titanium isopropoxide (TTIP) and O_2 as the titanium and oxygen sources, respectively. During the deposition, the reaction chamber was maintained at 250 °C. The growth rate is 0.51 Å/cycle, and 700 cycles were carried out to deposit 35.7 nm. One complete reaction cycle was composed of the following steps: (i) TTIP dosing for 2 s; (ii) TTIP purging for 3 s by Ar at 200 sccm; (iii) O_2 plasma gas stabilization for 500 ms; (iv) O_2 plasma for 3 s with RF power at 300 W; (v) plasma purging for 2 s by Ar at 150 sccm. After growth, the TiO_2 film was annealed at 450 °C for 2 h in a furnace.

Deposition of HfO_2 Film. The HfO_2 is deposited on TiO_2 film by ALD process using tetrakis(ethylmethylamino)hafnium (TEMAH) and O_2 as the hafnium and oxygen sources, respectively. During the deposition, the reaction chamber was maintained at 290 °C. One complete reaction cycle was composed of the following: (i) TEMAH dosing for 1 s; (ii) TEMAH purging for 3 s by Ar; (iii) pumping for 3 s; (iv) O_2 stabilization for 2 s; (v) O_2 plasma for 3 s with RF power 250 W; (vi) purging for 2 s by Ar. 36 cycles was used to deposit about 4 nm thick HfO_2 film with a growth rate of 1.13 Å/cycle.

Deposition of Al_2O_3 Film. The Al_2O_3 film is also deposited on TiO_2 film by ALD process using trimethylaluminum (TMA) and O_2 as the aluminum and oxygen sources, respectively. During the deposition, the reaction chamber was maintained at 300 °C. One complete reaction cycle was composed of the following: (i) TMA dosing for 20 ms; (ii) TMA purging for 1 s by Ar; (iii) O_2 stabilization for 500 ms; (iv) O_2 plasma for 2 s with RF power 300 W; (v) purging for 1 s by Ar gas. 45 cycles were used to deposit about 4 nm thick Al_2O_3 film with a growth rate of 0.88 Å/cycle.

Absorption of MBA Molecules. The prepared TiO_2 (and TiO_2/Al_2O_3, TiO_2/HfO_2) film was immersed in an MBA/ethanol solution (10^{-3} M) for 2 h. Subsequently, MBA molecules were fixed on the surface of the TiO_2 (and Al_2O_3, HfO_2) film through the carboxyl group. Thus, the ALD-TiO_2/MBA (and TiO_2/Al_2O_3/MBA, TiO_2/HfO_2/MBA) assembly was obtained.

Deposition of Al_2O_3 Film by E-Beam Evaporation. The Al_2O_3 layer in TiO_2/MBA/Al_2O_3 assembly was deposited by e-beam evaporation process at room temperature. The thickness of Al_2O_3 layer was set to 4 nm with a deposition rate of 0.5 Å/s. During deposition, the reaction chamber was maintained at 40 mTorr.

Deposition of Ag Island Film. The Ag island film in the TiO_2/MBA/Ag (TiO_2/Al_2O_3/MBA/Ag, TiO_2/HfO_2/MBA/Ag, and TiO_2/MBA/Al_2O_3/Ag) is deposited by e-beam evaporation at room temperature. The thickness of Ag island film was set to 10 nm with a deposition rate of 0.5 Å/s. The whole assembly process is schematically shown in Figure 1.

Instruments. The ALD process was conducted with an OXFORD FlexAL ALD (thermal and plasma) cluster system. The PVD process was conducted with Intelvac EB-PVD

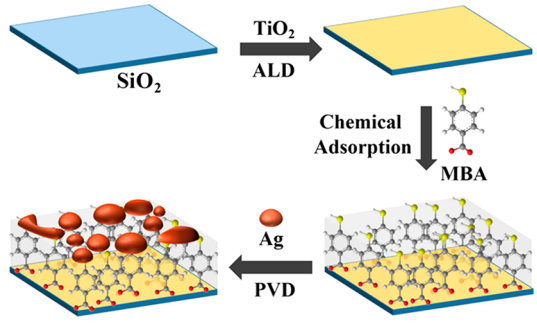

Figure 1. Schematic diagram of the preparation process of the TiO_2/MBA/Ag system.

DOI: 10.1021/acs.jpcc.7b10086
J. Phys. Chem. C 2017, 121, 26939−26948

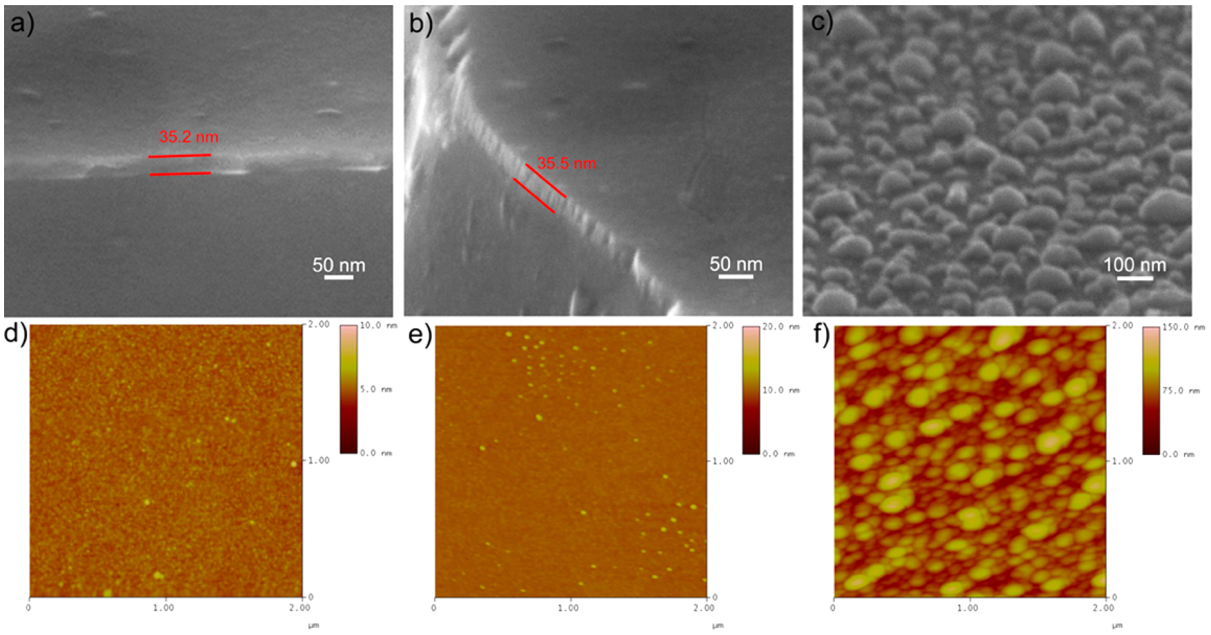

Figure 2. SEM and AFM images of TiO_2 (a, d), TiO_2/MBA (b, e), and TiO_2/MBA/Ag (c, f) systems.

equipment. Field emission scanning electron microscope (FE-SEM) (Zeiss UltraPlus) and atomic force microscopy (AFM) (Dimension 3100) were conducted to investigate the morphology of different systems. The UV−vis absorption spectra were obtained on a UV-2501PC spectrometer. The Raman spectra were collected at room temperature from a Renishaw ramascope dual-wavelength micro-Raman spectrometer. The resolution of Raman shift is 0.5 wavenumbers. A 633 nm laser was used as the excitation source, and a 50× objective lens was used to focus the laser beam. In all SERS measurements, the laser power was fixed to 2.3 mW/cm^2 with two times 10 s accumulations.

RESULTS AND DISCUSSION

Analysis of the TiO_2/MBA and TiO_2/MBA/Ag Systems. *Morphology Analysis.* Figure 2 shows the SEM and AFM images of TiO_2, TiO_2/MBA, and TiO_2/MBA/Ag systems. It can be seen from Figure 2a that the TiO_2 film is a thin layer with a thickness of 35.2 nm. The AFM image in Figure 2d is used to characterize the surface roughness of the TiO_2 film. The root-mean-square (RMS) value of the surface roughness for the as-grown TiO_2 film with a scanning size of 2 μm × 2 μm is 0.194 nm. Thus, the TiO_2 deposited with ALD is a highly flat film with a uniform thickness. Because the absorbed MBA molecules are only a very thin monolayer on the surface, the morphology of the ALD-TiO_2/MBA assembly shows little change after adsorption of MBA (Figure 2b,e). As Figure 2c,f shows, the Ag island film coated by e-beam evaporation is not smooth but has a random oblate spheroidal array nanostructure.

Measurement of the UV−Vis Spectra. Figure 3 shows the UV−vis absorption spectra of the TiO_2, TiO_2/MBA, and TiO_2/MBA/Ag systems between 200 and 900 nm wavelength. The TiO_2 film shows a band-edge absorption around 395 nm (3.14 eV), which is close to the reported value 3.2 eV. After the absorption of MBA molecules, there is a weak increase in the absorbance between 350 and 500 nm wavelength, which can be ascribed to a new CT complex formed between MBA molecules and TiO_2 substrate.[24] Compared with previous

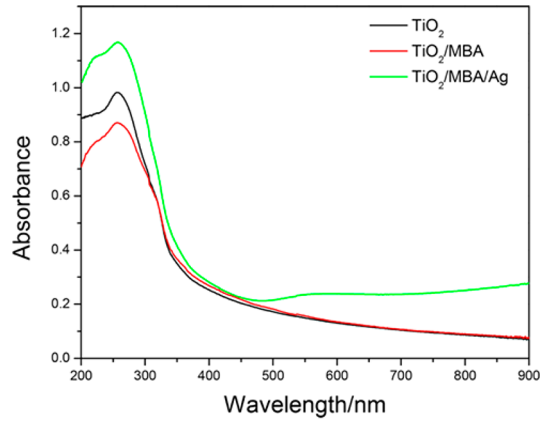

Figure 3. UV−vis absorption curves of the TiO_2, TiO_2/MBA, and TiO_2/MBA/Ag systems.

literatures, this absorbance increase is much weaker due to the poor adsorption capacity of TiO_2 film. After introducing Ag island film, the system shows a strong absorption between 500 and 900 nm wavelength which is assigned to SPR absorbance of the Ag film. Another evident change is the increase between 200 and 350 nm wavelength, which is usually ascribed to the transitions between the valence band and conduction band of TiO_2. The UV−vis absorption spectrum of Ag island film deposited on SiO_2 is shown in Figure.S1 in which a weak absorption peak is observed between 200 and 350 nm wavelength. Also in previous reports,[25,26] similar enhancements between 200 and 350 nm wavelength are observed in other noble metal/TiO_2 heterostructures, which is attributed to the interaction between the metal and semiconductor. Thus, we deduced both the absorption of Ag and interaction between the metal and semiconductor contribute to the absorption increase between 200 and 350 nm wavelength. With UV−vis spectra, it can be concluded that the CT system TiO_2/MBA/Ag is fabricated successfully.

SERS Analysis in the TiO_2/MBA and TiO_2/MBA/Ag Systems. Figure 4 shows the SERS spectra (at 633 nm) collected from

DOI: 10.1021/acs.jpcc.7b10086
J. Phys. Chem. C 2017, 121, 26939−26948

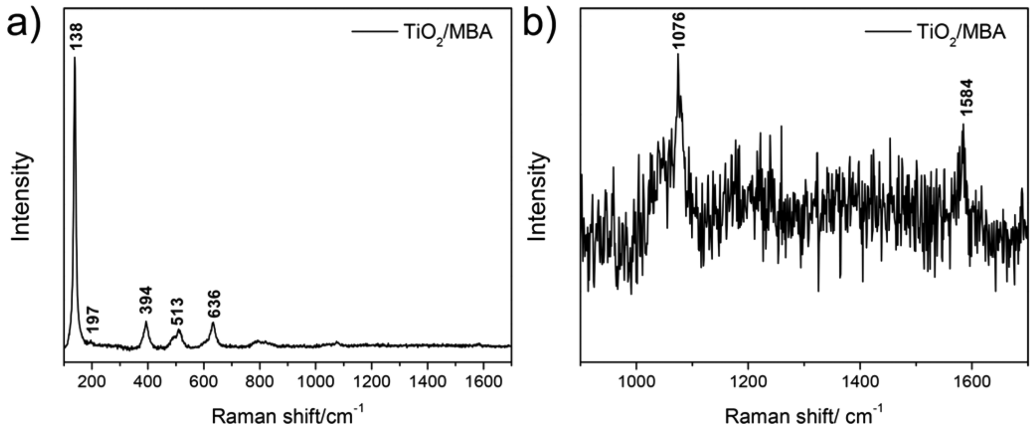

Figure 4. (a) SERS spectra collected from the TiO_2/MBA system at 633 nm excitation and (b) enlarged SERS spectra between 900 and 1700 cm^{-1}.

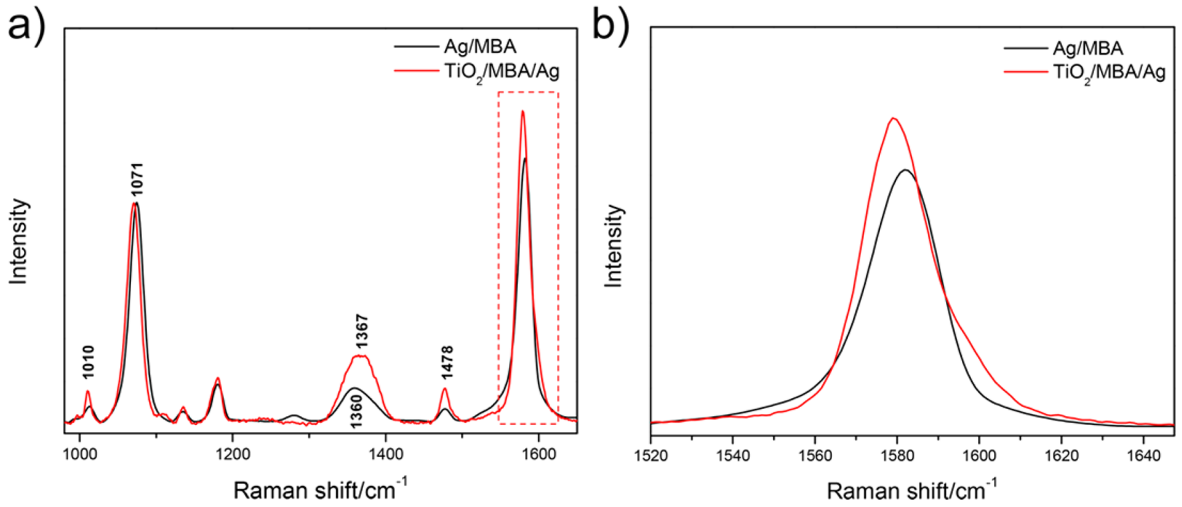

Figure 5. (a) SERS spectra of the MBA molecules in the TiO_2/MBA/Ag and Ag/MBA assemblies at 633 nm excitation. (b) Enlarged SERS spectra between 1520 and 1647 cm^{-1}.

TiO_2/MBA system. As Figure 4a shows, the Raman modes at 138, 197, 394, 513, and 636 cm^{-1} are assigned as E_g, E_g, B_{1g}, A_{1g} (or B_{1g}), and E_g modes in anatase phase, respectively.[27] Then, the SERS spectra between 1000 and 1650 cm^{-1} is enlarged in Figure 4b where the SERS signal of MBA molecules is observed. Compared with TiO_2–NPs/MBA system in previous reports, the SERS signal of ALD–TiO_2/MBA is relatively weak.

We also calculate the enhancement factor (EF) of the fabricated ALD–TiO_2 film with its definition[28]

$$EF = (I_{surf}/N_{surf})/(I_{bulk}/N_{bulk})$$

A value of about 1.1×10^3 was obtained for the EF of our ALD–TiO_2 film, which is lower than the value reported previously (3.5×10^3).[29] The calculation process is presented in the Supporting Information. The SERS effect of TiO_2 NPs is first observed in 2008 by Yang et al., which is attributed to the charge-transfer process between surface state energy level and LUMO of the adsorbed molecules. Thus, we deduce that two factors can account for the weaker enhancement effect of ALD-TiO_2 film: (i) The 2D TiO_2 film has less surface area than spherical TiO_2 NPs, which leads to poor adsorption capacity. Thus, fewer probe molecules on TiO_2 film are detected under the objective lens of SERS equipment. (ii) ALD deposition of a thin TiO_2 layer significantly improved the film uniformity, which leads to lower defect density as well as weaker SERS enhancement effect. The XPS in Figure S3 shows the higher O/Ti ratio in ALD–TiO_2 film compared with TiO_2 NPs, which is in accordance with our speculation. Additionally, compared with TiO_2 NPs, changes of Raman bands also confirm low defect density in ALD–TiO_2 film (Figure S4)

The SERS spectra of the MBA molecules in the TiO_2/MBA/Ag and Ag/MBA assemblies at 633 nm excitation are compared in Figure 5. Table 1 shows the assignment of bands in MBA molecules in the Ag/MBA system.

Table 1. Wavenumbers and Assignments of Bands in the SERS Spectrum of MBA Molecule[30,31]

wavenumbers (cm^{-1})	band assignments[a]	species
1010	in-plane ring breathing mode 1[b] + ν(CO)	b2
1071	in-plane ring breathing mode 1[b] + ν(CS)	a1
1360	β(OH) + ν(C-ph) + in-plane mode ν(CC) 19a[b] + asymmetry $\nu(CO_2)$	b2
1478	in-plane β(CH) mode 15[b]	b2
1572	ν(CC) + in-plane β(CH) mode 9b[b]	b2
1585	in-plane β(CH) mode 9a[b]	a1

[a] ν, stretching; β, bending. For ring vibrations, the corresponding vibrational modes of benzene and the symmetry species under C_{2v} symmetry are indicated. [b] The Wilson notation is employed.

DOI: 10.1021/acs.jpcc.7b10086
J. Phys. Chem. C 2017, 121, 26939–26948

For clarity, the SERS spectra have been normalized with the band at 1071 cm^{-1}. As Figure 5a shows, after the Ag/MBA system contact with TiO_2 layer, some changes in the relative intensity and peak position of different peaks are observed. First, the band at 1071 cm^{-1} (enlarged in Figure S5) shows a small shift in peak position with no width change, which can be ascribed to the change in the surrounding of MBA molecules. Also, the bands at 1010 and 1478 cm^{-1}, which are assigned to nontotally vibration mode, display an evident increase in the intensity of the SERS spectrum. Another noteworthy change is the enhancement of the peak at 1360 cm^{-1} in ALD−TiO_2/MBA/Ag system (Figure 5a). The peak at 1360 cm^{-1}, ascribed to the b2 mode, arises from the combination or overlap of O−H bending, the carboxyl carbon, and aromatic carbon stretching, 19a (the Wilson notation), coupled with CO_2 asymmetric stretch. According to previous reports,[32,33] the band at about 1580 cm^{-1} (in the red dashed box) is an overlap result of two SERS bands: totally symmetric in-plane C−H bending mode at 1585 cm^{-1} and non-totally symmetric in-plane C−H bending mode coupling with C−C stretching mode at 1572 cm^{-1}. As Figure 5b shows, the peak shape of this composite band in the TiO_2/MBA/Ag system becomes more symmetrical than that in Ag/MBA after contacting with TiO_2. This phenomenon can be attributed to the change in intensity ratio between bands at 1572 and 1585 cm^{-1} where the former band intensity is enhanced. Then, we can conclude that almost all the changes in TiO_2/MBA/Ag system (except the shift at 1077 cm^{-1}) are caused by the selective enhancement of b2-type vibrational mode.

According to the CT model of Lombardi,[19] only totally symmetric vibrational modes of the probe molecules are expected to be enhanced via the Franck−Condon contribution, and the Herzberg− Teller effect can enhance both totally and non-totally symmetric vibrational signatures in the SERS spectra of the probe molecule. That is, the b2 mode can be selectively enhanced by the CT mechanism through the Herzberg−Teller contribution. Thus, it can be deduced that the selective enhancements of the b2 mode may come from a new CT process that occurs between TiO_2, MBA molecules, and Ag.

Additionally, it is worth noting that the interaction between TiO_2, MBA molecules, and Ag also has an impact on the TiO_2 phonon vibrational mode. For clarity, the bands are normalized at 137 cm^{-1}. Then we can observe in Figure 6 that the band at 137 cm^{-1} (E_g) broadens and shifts toward higher wavenumbers 139.5 cm^{-1} in the TiO_2/MBA/Ag system. This phenomenon can be ascribed to CT process in the TiO_2/MBA/Ag system, which further influences the phonon density of states in anatase TiO_2 as well as the TiO_2 phonon vibrational mode in Raman spectra. A similar change in the Raman spectra of TiO_2 is also reported in other paper where this phenomenon is ascribed to the interaction between metal and semiconductor.[34]

Analysis of the TiO_2/HfO_2/MBA/Ag System. To confirm the changes in SERS coming from the new CT process in TiO_2/MBA/Ag, we insert a layer of wide-bandgap oxide to separate the TiO_2 layer from whole CT system. Because of its high dielectric constant and relatively high thermal stability, HfO_2 has been extensively used as a high-κ dielectric material for field effect transistors.[35] For the sake of uniformity, the ALD technique is chosen to deposit a 4 nm layer of HfO_2 on TiO_2 film as an isolation layer. Figure S6 show the AFM and SEM images of TiO_2/HfO_2 assembly. The RMS value of the surface roughness for the as-grown TiO_2/HfO_2 with a scanning size of 2 μm × 2 μm is 0.354 nm, which indicates the high uniformity of HfO_2 layer.

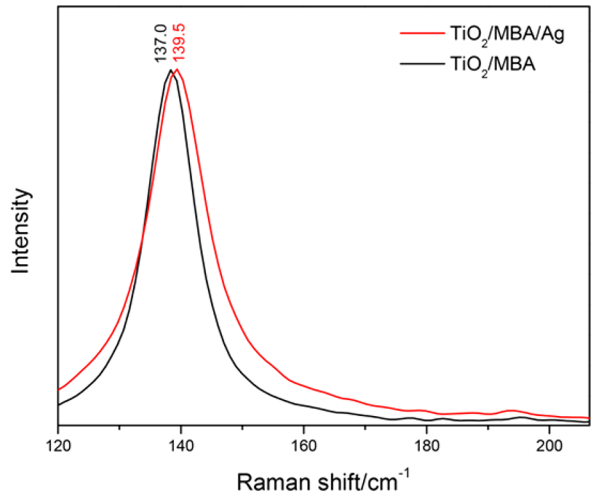

Figure 6. Raman spectra of TiO_2 in the TiO_2/MBA and TiO_2/MBA/Ag systems at 633 nm excitation.

UV−Vis Spectra Measurement of the TiO_2/HfO_2/MBA/Ag System. Figure 7 shows the UV−vis absorption spectra of

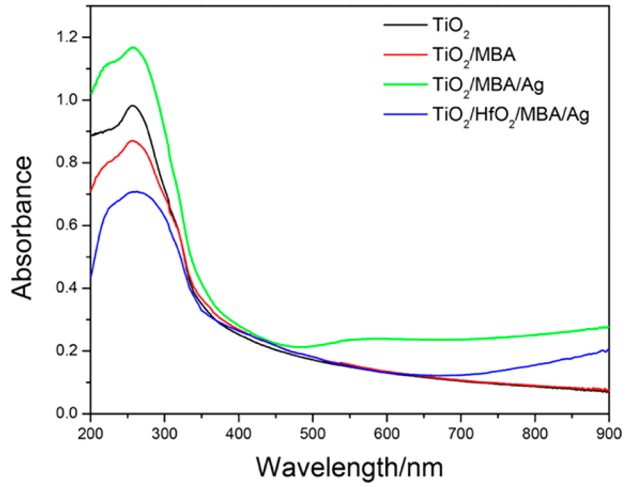

Figure 7. UV−vis absorption spectra of the TiO_2, TiO_2/MBA, TiO_2/MBA/Ag, and TiO_2/HfO_2/MBA/Ag systems.

TiO_2, TiO_2/MBA, TiO_2/MBA/Ag, and TiO_2/HfO_2/MBA/Ag systems. After inserting HfO_2 layer into the TiO_2/MBA/Ag, there is a decrease in the absorbance between 200 and 350 nm wavelength, which can prove the interruption of CT process between TiO_2, MBA molecules, and Ag; the LSPR absorbance of the Ag film shows an evident red-shift. According to the SEM images, the Ag islands in the TiO_2/MBA/Ag (Figure 2c) and TiO_2/HfO_2/MBA/Ag systems (Figure S7) have similar morphological features. According to Gans scattering theory,[36,37] the SPR resonance will shift as the media permittivity around the metal nanostructures changes. In our case, the HfO_2 has a different permittivity from air or TiO_2 layer, and thus the shift of Ag SPR resonance is observed in Figure 7. In conclusion, it can be speculated from UV−vis spectra that the CT process in TiO_2/MBA/Ag is weakened by the inserting of an HfO_2 layer with ALD.

DOI: 10.1021/acs.jpcc.7b10086
J. Phys. Chem. C 2017, 121, 26939−26948

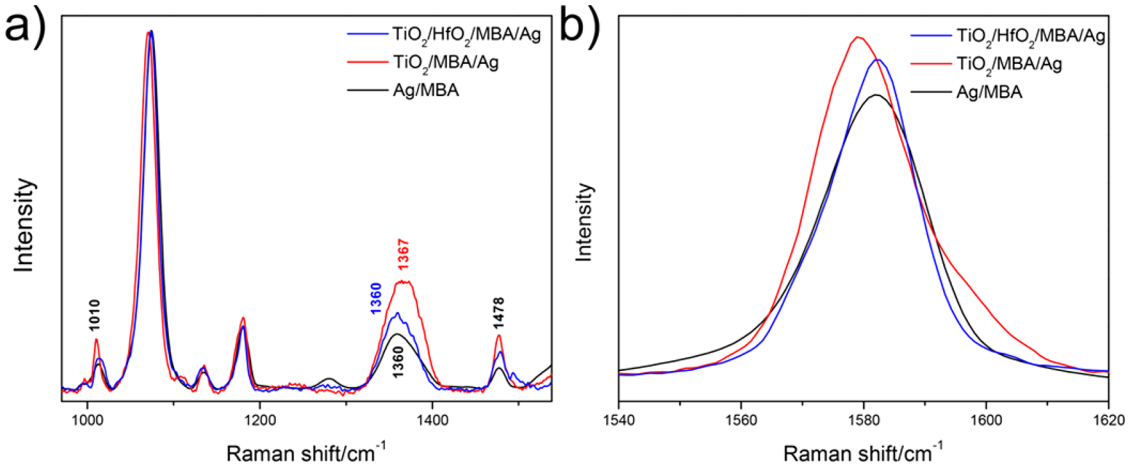

Figure 8. (a) SERS spectra of the MBA molecules in the $TiO_2/HfO_2/MBA/Ag$, $TiO_2/MBA/Ag$, and Ag/MBA assemblies at 633 nm excitation. (b) Enlarged SERS spectra between 1540 and 1620 cm^{-1}.

SERS Analysis of the $TiO_2/HfO_2/MBA/Ag$ System. The SERS spectra of the Ag/MBA, $TiO_2/MBA/Ag$, and $TiO_2/HfO_2/MBA/Ag$ systems are compared in Figure 8. For clarity, the Raman spectra have been normalized with the band at 1071 cm^{-1}. As Figure 8a shows, after inserting HfO_2 layer, the bands at 1010, 1360, and 1478 cm^{-1}, which are enhanced in $TiO_2/MBA/Ag$, display an evident decrease. The composite bands at about 1580 cm^{-1} are enlarged in Figure 8b. The isolation effect of HfO_2 layer leads to the similarity of the 1580 cm^{-1} composite band shape in Ag/MBA and $TiO_2/HfO_2/MBA/Ag$ systems where Ag plays the sole role in SERS enhancement. Compared with that in $TiO_2/MBA/Ag$, the shape of the composite bands at ~1580 cm^{-1} turns back to be asymmetrical, which indicates a decrease of the band at 1572 cm^{-1} (b2). It can be concluded that the inset of HfO_2 layer leads to the interruption of the CT process between TiO_2, MBA molecules, and Ag film which can be further reflected in SERS spectra through the decrease in the intensity of b2-type bands. We also chose another high dielectric constant oxide Al_2O_3 as an isolation layer (4 nm) to further verify the obtained phenomenon as well as the validity of SERS in CT investigation. In Figure S8, the b2-type bands in $TiO_2/Al_2O_3/MBA/Ag$ show the same trend as that in $TiO_2/HfO_2/MBA/Ag$ system, which further proves the correlation between CT process and the intensity of b2-type bands in SERS spectra.

Another noteworthy phenomenon is the changes in TiO_2 phonon vibrational mode after inserting HfO_2. It can be seen from Figure 9 that the band at 137 cm^{-1} (E_g) broadens and shifts toward higher wavenumbers (139.5 cm^{-1}) in the $TiO_2/MBA/Ag$ system. After inserting HfO_2 layer, the band at 139.5 cm^{-1} in the $TiO_2/MBA/Ag$ shifts back to 138.5 cm^{-1} in the $TiO_2/HfO_2/MBA/Ag$ system. Also, as we expected, as the shift of the band at 137 cm^{-1}, the bandwidth is narrowed in the $TiO_2/HfO_2/MBA/Ag$ system. Thus, it can be deduced that in the $TiO_2/HfO_2/MBA/Ag$ system the impact of CT process on TiO_2 phonon vibrational mode is interrupted by inserting the HfO_2 layer.

Charge-Transfer Analysis of the $TiO_2/MBA/Ag$ and $TiO_2/HfO_2/MBA/Ag$ Systems. To explain the extra enhancement in the $TiO_2/MBA/Ag$ and $TiO_2/HfO_2/MBA/Ag$ assemblies, mechanistic models for the CT process are proposed in Figure 10. It is widely believed that referring to the vacuum level, the Fermi level of Ag is situated at −4.26 eV. The highest occupied

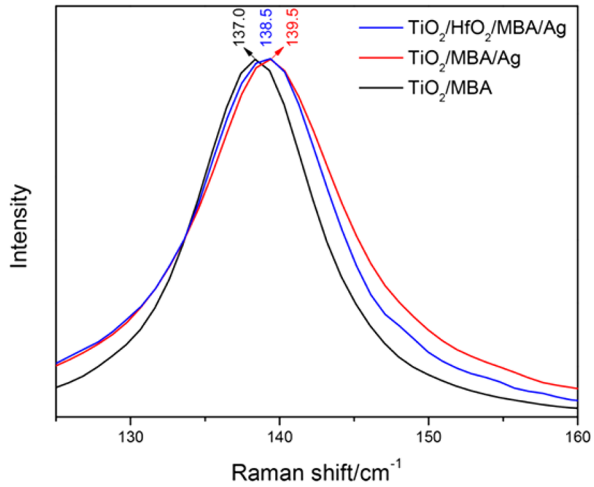

Figure 9. Raman band of TiO_2 in the $TiO_2/HfO_2/MBA/Ag$, $TiO_2/MBA/Ag$, and TiO_2/MBA assemblies at 633 nm excitation.

molecular orbital (HOMO) and the lowest unoccupied molecular orbital (LUMO) levels of MBA molecules are situated at −6.24 and −1.68 eV, respectively. The CBs and VBs of TiO_2 are situated at −4.00 eV and −7.20 eV, respectively. As illustrated schematically in Figure 10a, in $TiO_2/MBA/Ag$, given the high energy barrier, the incident laser does not have enough energy to transfer the excited electrons from the Fermi level of Ag to the LUMO of MBA molecules. The existence of TiO_2 provides a new CT path in which the excited electron generated at the Fermi level of Ag transfers to the CB level of semiconductor TiO_2 under 633 nm excitation (1.96 eV). Thus, we observed the selectively enhanced b2-type mode in the $TiO_2/MBA/Ag$ system.

The CBs and VBs of the HfO_2 layer are situated at −2.00 and −8.4 eV, respectively. As schematically illustrated in Figure 10b, the energy barrier between the Fermi level of Ag and the CB level of HfO_2 is 2.26 eV. In this case, the incident laser photon does not have enough energy to overcome the energy barrier. Meanwhile, according to Song's report, electron tunneling also hardly occurs at the 4 nm thickness of HfO_2 gap.[38] Thus, the CT process is interrupted in the $TiO_2/HfO_2/MBA/Ag$, which leads to the intensity decrease of b2-type bands after inserting HfO_2 layer.

DOI: 10.1021/acs.jpcc.7b10086
J. Phys. Chem. C 2017, 121, 26939−26948

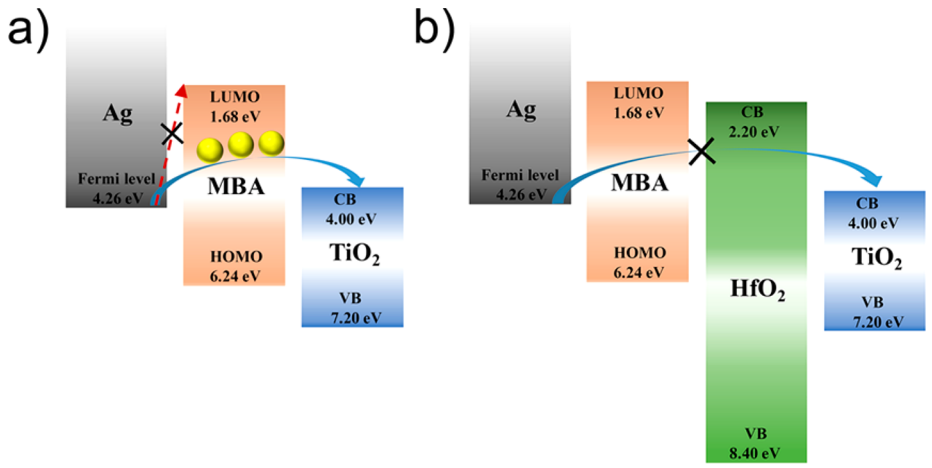

Figure 10. CT mechanism in TiO_2/MBA/Ag and TiO_2/HfO_2/MBA/Ag assemblies.

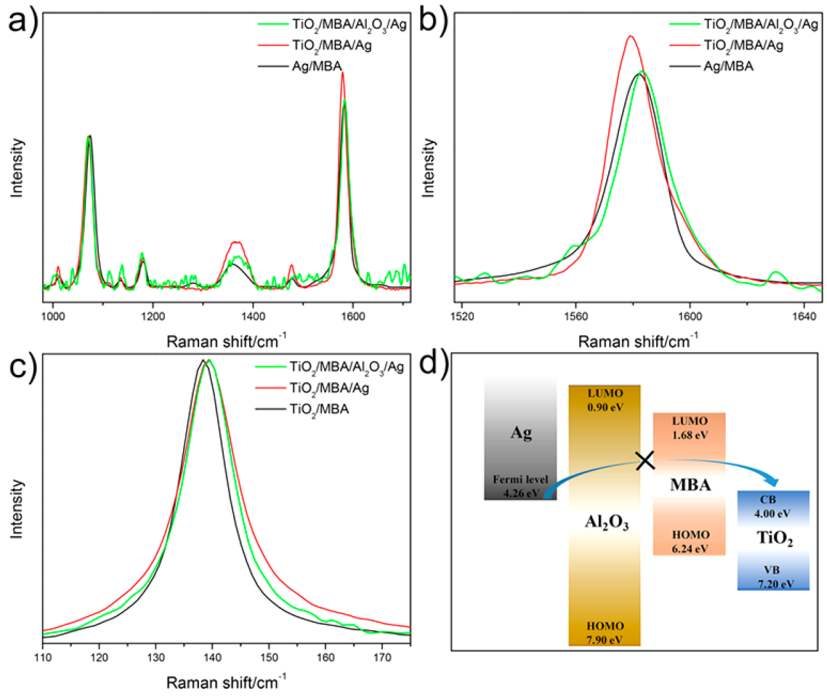

Figure 11. (a) SERS spectra of the MBA molecules in the TiO_2/MBA/Al_2O_3/Ag, TiO_2/MBA/Ag, and Ag/MBA assemblies at 633 nm excitation. (b) Enlarged SERS spectra between 1517 and 1646 cm^{-1}. (c) Band of TiO_2 Raman spectra in the TiO_2/MBA/Al_2O_3/Ag, TiO_2/MBA/Ag, and Ag/MBA assemblies. (d) CT mechanism in the TiO_2/MBA/Al_2O_3/Ag assembly.

Analysis of the TiO_2/MBA/Al_2O_3/Ag System. With the TiO_2/MBA/Ag assembly, we observed the CT process between TiO_2, MBA, and Ag by the selectively enhancement of b2-type mode. Given the location of energy level, there is a CT process from the Fermi level of Ag to the CB of TiO_2. The inserting of HfO_2 hinders the migration of the electrons to TiO_2. To further confirm the Ag-to-molecule-to-TiO_2 CT path, we also investigated the SERS signal of MBA molecules in the TiO_2/MBA/Al_2O_3/Ag system. Because the high temperature condition in ALD process can lead to decomposition of MBA molecules, we chose e-beam evaporation to insert a 4 nm layer of Al_2O_3 to cut the CT path by separating Ag from the TiO_2/MBA system. In the TiO_2/MBA/Al_2O_3/Ag system, because the thickness of Al_2O_3 is just 4 nm, the SERS signal of MBA molecules mainly comes from EM of Ag island film.[18] As we expect, due to the disruption of CT process, the bands assigned to non-totally vibrational mode in the MBA SERS spectra show similar changes as that in TiO_2/HfO_2/MBA/Ag. As Figure 11a shows, the bands at 1010, 1360, and 1478 cm^{-1} show distinct decrease in intensity. Meanwhile, it can be observed in Figure 11b that the composite bands become asymmetrical again which indicates the decrease in the intensity of b2-type band at 1572 cm^{-1}. Additionally, the Raman spectra of TiO_2 in the TiO_2/MBA/Al_2O_3/Ag system also show some similar changes to the TiO_2/HfO_2/MBA/Ag system. As Figure 11c shows, the peak at 139.5 cm^{-1} shifts toward lower wavenumber and narrows after inserting Al_2O_3 layer which also indicates an interruption of the CT process between TiO_2, MBA, and Ag.

The energy level diagram is drawn to show the involved CT mechanism of TiO_2/MBA/Al_2O_3/Ag in Figure 11d. The CBs and VBs of the Al_2O_3 layer is situated at −0.9 eV and −7.9 eV, respectively.[39] The energy barrier between the Fermi level of

DOI: 10.1021/acs.jpcc.7b10086
J. Phys. Chem. C 2017, 121, 26939−26948

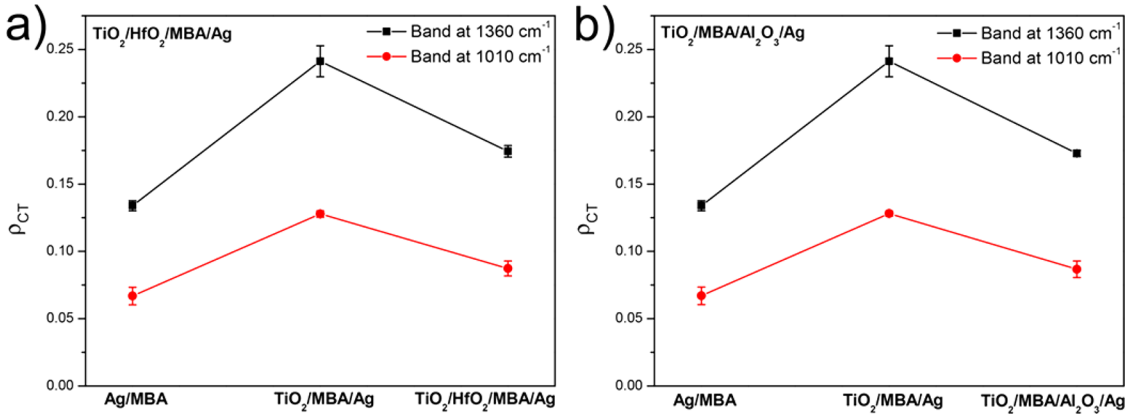

Figure 12. Variation trend of ρ_{CT} in Ag/MBA, TiO_2/MBA/Ag, TiO_2/HfO_2/MBA/Ag, and TiO_2/MBA/Al_2O_3/Ag assemblies at 633 nm excitation.

Ag and the CB level of Al_2O_3 is 3.16 eV. In this case, the electrons in Ag cannot get enough energy from incident laser photon to overcome the energy barrier, which inhibits the transition of excited electrons in Ag and leads to the interruption of the interfacial CT process in the TiO_2/MBA/Al_2O_3/Ag assembly. Thus, the selective enhancements of b2-type mode cannot be observed. The SERS spectra of the TiO_2/MBA/Al_2O_3/Ag system provide more evidence for the existence of the CT process from Ag to TiO_2 layer.

Degree of Charge Transfer in Different Systems. We utilized the bands at 1367 and 1010 cm^{-1} to measure degree of CT (ρ_{CT}) in the Ag/MBA, TiO_2/MBA/Ag, TiO_2/MBA/Al_2O_3/Ag, and TiO_2/HfO_2/MBA/Ag assemblies, which is helpful in understanding the CT processes for different systems. The ρ_{CT} can be estimated according to the following equation:[21]

$$\rho_{CT} = \frac{I_{b2}/I_{a1}}{1 + I_{b2}/I_{a1}}$$

Here, the intensity of the strong a1 line at 1071 cm^{-1} are used as I_{a1}. Figure 12 shows the variation trend of ρ_{CT} in the Ag/MBA, TiO_2/MBA/Ag, TiO_2/HfO_2/MBA/Ag, and TiO_2/MBA/Al_2O_3/Ag assemblies at 633 nm excitation. In Ag/MBA, the ρ_{CT} is low, which is in accordance with the proposed mechanism in Figure 10a. After in contact with TiO_2, the ρ_{CT} becomes higher due to the CT process that occurs between the Fermi level of Ag and the CB level of TiO_2 film. However, the insertion of HfO_2 and Al_2O_3 leads to a decrease in the ρ_{CT} value because of the interruption of the CT process. The variation trend of ρ_{CT} further confirms our proposed CT mechanism.

From above, it can be deduced that with the highly ordered CT models fabricated by ALD and e-beam evaporation, the CT process in metal-molecule-semiconductor system can be observed through the increase or decrease in intensity of b2-type bands in SERS. Thus, with the SERS technique, we can obtain a better understanding of the CT involved in many optoelectronic devices.

CONCLUSION

In this work, the 2D semiconductor−molecule−metal system TiO_2/MBA/Ag has been fabricated by ALD and e-beam evaporation technique to study the interfacial CT process with SERS. Comparing with Ag/MBA system, b2-type bands at 1010, 1360, and 1478 cm^{-1} are significantly enhanced in the TiO_2/MBA/Ag system, which can be attributed to the CT process between TiO_2, MBA, and Ag island film. Meanwhile, the impact of the involved CT process TiO_2 phonon vibrational mode is also observed in the Raman spectra. After inserting the wide-bandgap HfO_2 layer into the TiO_2/MBA/Ag system, we observed opposite changes in the SERS signal of MBA molecules and Raman spectra of TiO_2 phonon vibrational mode. Thus, the significant evidence of the CT process are archived with the help of advanced fabrication skill and SERS technique. Meanwhile, the possible CT mechanisms and the charge-transfer degree in different systems are discussed. Finally, to confirm the proposed mechanism, the SERS signal of MBA molecules in the TiO_2/MBA/Al_2O_3/Ag system is also investigated. We hope this work not only promote the revolution of CT model fabrication skills but also broaden the application scope of SERS technique to the area of interfacial CT investigation.

ASSOCIATED CONTENT

Supporting Information

The Supporting Information is available free of charge on the ACS Publications website at DOI: 10.1021/acs.jpcc.7b10086.

(a) UV−vis spectrum of Ag island film on SiO_2; (b) calculation process of EF; (c) XPS analysis of TiO_2 film and TiO_2 NPs; (d) Raman spectra of TiO_2 particles and ALD TiO_2 film; (e) enlarged Raman spectra between 980 and 1180 cm^{-1}; (f) the AFM images of TiO_2/HfO_2 assembly; (g) SEM image of TiO_2/HfO_2/MBA/Ag system; (h) SERS spectra of the MBA molecules in the TiO_2/Al_2O_3/MBA/Ag, TiO_2/MBA/Ag, and Ag/MBA assemblies between 980 and 1520 cm^{-1} at 633 nm excitation (PDF)

AUTHOR INFORMATION

Corresponding Authors

*Tel +86-431-85168473; Fax +86-431-85193421; e-mail zhaob@mail.jlu.edu.cn (B.Z.).

*Tel +1-(519) 888 4567 ext 38754; Fax +1- (519) 746 3077; e-mail bcui@uwaterloo.ca (B.C.).

ORCID

Bing Zhao: 0000-0002-9559-589X

Notes

The authors declare no competing financial interest.

ACKNOWLEDGMENTS

The research was supported by the National Natural Science Foundation (Grants 21273091, 21221063, 21327803,

DOI: 10.1021/acs.jpcc.7b10086
J. Phys. Chem. C 2017, 121, 26939−26948

21411140235, and 21073072) of the P. R. China; the 111 project (B06009); and the Science and Technology Development Program of Jilin Province (20110338 and 20130305005GX).

REFERENCES

(1) Wang, W.; Lee, T.; Kamdar, M.; Reed, M. A.; Stewart, M. P.; Hwang, J. J.; Tour, J. M. Electrical Characterization of Metal-Molecule-Silicon Junctions. *Superlattices Microstruct.* **2003**, *33*, 217−226.
(2) Hsu, J. W. P.; Loo, Y. L.; Lang, D. V.; Rogers, J. A. Nature of Electrical Contacts in a Metal-Molecule-Semiconductor System. *J. Vac. Sci. Technol., B: Microelectron. Process. Phenom.* **2003**, *21*, 1928.
(3) Haick, H.; Ghabboun, J.; Niitsoo, O.; Cohen, H.; Cahen, D.; Vilan, A.; Hwang, J.; Wan, A.; Amy, F.; Kahn, A. Effect of Molecular Binding to a Semiconductor on Metal/Molecule/Semiconductor Junction Behavior. *J. Phys. Chem. B* **2005**, *109*, 9622−9630.
(4) Scott, A.; Hacker, C. A.; Janes, D. B. In Situ Structural Characterization of Metal−Molecule−Silicon Junctions Using Backside Infrared Spectroscopy. *J. Phys. Chem. C* **2008**, *112*, 14021−14026.
(5) Whitney, A. V.; Elam, J. W.; Zou, S.; Zinovev, A. V.; Stair, P. C.; Schatz, G. C.; Van Duyne, R. P. Localized Surface Plasmon Resonance Nanosensor: A High-Resolution Distance-Dependence Study Using Atomic Layer Deposition. *J. Phys. Chem. B* **2005**, *109*, 20522−20528.
(6) Zhang, W.; Dong, J. C.; Li, C. Y.; Chen, S.; Zhan, C.; Panneerselvam, R.; Yang, Z. L.; Li, J. F.; Zhou, Y. L. Large Scale Synthesis of Pinhole-Free Shell-Isolated Nanoparticles (SHINERS) Using Improved Atomic Layer Deposition (ALD) Method for Practical Applications. *J. Raman Spectrosc.* **2015**, *46*, 1200−1204.
(7) Greiner, M. T.; Chai, L.; Helander, M. G.; Tang, W. M.; Lu, Z. H. Metal/Metal-Oxide Interfaces: How Metal Contacts Affect the Work Function and Band Structure of MoO_3. *Adv. Funct. Mater.* **2013**, *23*, 215−226.
(8) Sauer, C.; Wiessner, M.; Scholl, A.; Reinert, F. Observation of a Molecule-Metal Interface Charge Transfer Related Feature by Resonant Photoelectron Spectroscopy. *New J. Phys.* **2015**, *17*, 043016.
(9) Furube, A.; Du, L.; Hara, K.; Katoh, R.; Tachiya, M. Ultrafast Plasmon-Induced Electron Transfer from Gold Nanodots into TiO_2 Nanoparticles. *J. Am. Chem. Soc.* **2007**, *129*, 14852−14853.
(10) Fleischmann, M.; Hendra, P. J.; McQuillan, A. J. Raman Spectra of Pyridine Adsorbed at a Silver Electrode. *Chem. Phys. Lett.* **1974**, *26*, 163−166.
(11) Shaban, M.; Galaly, A. R. Highly Sensitive and Selective In-Situ SERS Detection of Pb^{2+}, Hg^{2+}, and Cd^{2+} Using Nanoporous Membrane Functionalized with CNTs. *Sci. Rep.* **2016**, *6*, 25307.
(12) Muehlethaler, C.; Considine, C. R.; Menon, V.; Lin, W.-C.; Lee, Y.-H.; Lombardi, J. R. Ultrahigh Raman Enhancement on Monolayer MoS_2. *ACS Photonics* **2016**, *3*, 1164−1169.
(13) Schedin, F.; Lidorikis, E.; Lombardo, A.; Kravets, V. G.; Geim, A. K.; Grigorenko, A. N.; Novoselov, K. S.; Ferrari, A. C. Surface-Enhanced Raman Spectroscopy of Graphene. *ACS Nano* **2010**, *4*, 5617−5626.
(14) Ngo, H. T.; Wang, H.-N.; Fales, A. M.; Vo-Dinh, T. Plasmonic SERS Biosensing Nanochips for DNA Detection. *Anal. Bioanal. Chem.* **2016**, *408*, 1773−1781.
(15) Tripp, R. A.; Dluhy, R. A.; Zhao, Y. Novel Nanostructures for SERS Biosensing. *Nano Today* **2008**, *3*, 31−37.
(16) Zaleski, S.; Wilson, A. J.; Mattei, M.; Chen, X.; Goubert, G.; Cardinal, M. F.; Willets, K. A.; Van Duyne, R. P. Investigating Nanoscale Electrochemistry with Surface- and Tip-Enhanced Raman Spectroscopy. *Acc. Chem. Res.* **2016**, *49*, 2023−2030.
(17) Qi, D.; Yan, X.; Wang, L.; Zhang, J. Plasmon-Free SERS Self-Monitoring of Catalysis Reaction on Au Nanoclusters/TiO_2 Photonic Microarray. *Chem. Commun.* **2015**, *51*, 8813−8816.
(18) Stiles, P. L.; Dieringer, J. A.; Shah, N. C.; Van Duyne, R. P. Surface-Enhanced Raman Spectroscopy. *Annu. Rev. Anal. Chem.* **2008**, *1*, 601−626.
(19) Lombardi, J. R.; Birke, R. L. A Unified Approach to Surface-Enhanced Raman Spectroscopy. *J. Phys. Chem. C* **2008**, *112*, 5605−5617.
(20) Sun, Z.; Wang, C.; Yang, J.; Zhao, B.; Lombardi, J. R. Nanoparticle Metal-Semiconductor Charge Transfer in ZnO/PATP/Ag Assemblies by Surface-Enhanced Raman Spectroscopy. *J. Phys. Chem. C* **2008**, *112*, 6093−6098.
(21) Richter, A. P.; Lombardi, J. R.; Zhao, B. Size and Wavelength Dependence of the Charge-Transfer Contributions to Surface-Enhanced Raman Spectroscopy in Ag/PATP/ZnO Junctions. *J. Phys. Chem. C* **2010**, *114*, 1610−1614.
(22) Wang, X.; Wang, Y.; Sui, H.; Zhang, X.; Su, H.; Cheng, W.; Han, X. X.; Zhao, B. Investigation of Charge Transfer in Ag/N719/TiO_2 Interface by Surface-Enhanced Raman Spectroscopy. *J. Phys. Chem. C* **2016**, *120*, 13078−13086.
(23) Wang, X.; Zhao, B.; Li, P.; Han, X. X.; Ozaki, Y. Charge Transfer at the TiO_2/N3/Ag Interface Monitored by Surface-Enhanced Raman Spectroscopy. *J. Phys. Chem. C* **2017**, *121*, 5145−5153.
(24) Yang, L.; Jiang, X.; Ruan, W.; Yang, J.; Zhao, B.; Xu, W.; Lombardi, J. R. Charge-Transfer-Induced Surface-Enhanced Raman Scattering on Ag-TiO_2 Nanocomposites. *J. Phys. Chem. C* **2009**, *113*, 16226−16231.
(25) Lin, Z.; Wang, X.; Liu, J.; Tian, Z.; Dai, L.; He, B.; Han, C.; Wu, Y.; Zeng, Z.; Hu, Z. On the Role of Localized Surface Plasmon Resonance in Uv-vis Light Irradiated Au/TiO(2) Photocatalysis Systems: Pros and Cons. *Nanoscale* **2015**, *7*, 4114−4123.
(26) Awate, S. V.; Deshpande, S. S.; Rakesh, K.; Dhanasekaran, P.; Gupta, N. M. Role of Micro-Structure and Interfacial Properties in the Higher Photocatalytic Activity of TiO_2-Supported Nanogold for Methanol-Assisted Visible-Light-Induced Splitting of Water. *Phys. Chem. Chem. Phys.* **2011**, *13*, 11329−11339.
(27) Ohsaka, T.; Izumi, F.; Fujiki, Y. Raman Spectrum of Anatase, TiO_2. *J. Raman Spectrosc.* **1978**, *7*, 321−324.
(28) Le Ru, E. C.; Blackie, E.; Meyer, M.; Etchegoin, P. G. Surface Enhanced Raman Scattering Enhancement Factors: A Comprehensive Study. *J. Phys. Chem. C* **2007**, *111*, 13794−13803.
(29) Xue, X.; Ji, W.; Mao, Z.; Mao, H.; Wang, Y.; Wang, X.; Ruan, W.; Zhao, B.; Lombardi, J. R. Raman Investigation of Nanosized TiO_2: Effect of Crystallite Size and Quantum Confinement. *J. Phys. Chem. C* **2012**, *116*, 8792−8797.
(30) Li, R.; Lv, H.; Zhang, X.; Liu, P.; Chen, L.; Cheng, J.; Zhao, B. Vibrational Spectroscopy and Density Functional Theory Study of 4-Mercaptobenzoic Acid. *Spectrochim. Acta, Part A* **2015**, *148*, 369−374.
(31) Wilson, E. B. The Normal Modes and Frequencies of Vibration of the Regular Plane Hexagon Model of the Benzene Molecule. *Phys. Rev.* **1934**, *45*, 706−714.
(32) Wang, Y.; Ji, W.; Sui, H.; Kitahama, Y.; Ruan, W.; Ozaki, Y.; Zhao, B. Exploring the Effect of Intermolecular H-Bonding: A Study on Charge-Transfer Contribution to Surface-Enhanced Raman Scattering of p-Mercaptobenzoic Acid. *J. Phys. Chem. C* **2014**, *118*, 10191−10197.
(33) Zhang, X.; Yu, Z.; Ji, W.; Sui, H.; Cong, Q.; Wang, X.; Zhao, B. Charge-Transfer Effect on Surface-Enhanced Raman Scattering (SERS) in an Ordered Ag Nps/4-Mercaptobenzoic Acid/TiO_2 System. *J. Phys. Chem. C* **2015**, *119*, 22439−22444.
(34) Stroyuk, O. L.; Dzhagan, V. M.; Kozytskiy, A. V.; Breslavskiy, A. Y.; Kuchmiy, S. Y.; Villabona, A.; Zahn, D. R. T. Nanocrystalline TiO_2/Au Films: Photocatalytic Deposition of Gold Nanocrystals and Plasmonic Enhancement of Raman Scattering from Titania. *Mater. Sci. Semicond. Process.* **2015**, *37*, 3−8.
(35) Gonzalez, G.; Kolosovas-Machuca, E. S.; Lopez-Luna, E.; Hernandez-Arriaga, H.; Gonzalez, F. J. Design and Fabrication of Interdigital Nanocapacitors Coated with HfO_2. *Sensors* **2015**, *15*, 1998−2005.
(36) Gans, R. Über Die Form Ultramikroskopischer Goldteilchen. *Ann. Phys.* **1912**, *342*, 881−900.
(37) Gans, R. Über Die Form Ultramikroskopischer Silberteilchen. *Ann. Phys.* **1915**, *352*, 270−284.

DOI: 10.1021/acs.jpcc.7b10086
J. Phys. Chem. C 2017, 121, 26939−26948

(38) Song, B.; Yao, Y.; Groenewald, R. E.; Wang, Y.; Liu, H.; Wang, Y.; Li, Y.; Liu, F.; Cronin, S. B.; Schwartzberg, A. M.; et al. Probing Gap Plasmons Down to Subnanometer Scales Using Collapsible Nanofingers. *ACS Nano* **2017**, *11*, 5836−5843.
(39) Chen, W.; Wu, Y.; Liu, J.; Qin, C.; Yang, X.; Islam, A.; Cheng, Y.-B.; Han, L. Hybrid Interfacial Layer Leads to Solid Performance Improvement of Inverted Perovskite Solar Cells. *Energy Environ. Sci.* **2015**, *8*, 629−640.

DOI: 10.1021/acs.jpcc.7b10086
J. Phys. Chem. C 2017, 121, 26939−26948